TECHNISCHE MECHANIK
an open access journal

journal homepage: www.ovgu.de/techmech

Tech. Mech., Vol. 43, Is. 2, (2023), 271–283

Received: 18.09.2023
Accepted: 08.12.2023
Available online: 08.12.2023

Improved modeling and design of soft robots using sensitivity analysis

Frederik Lamping[1], Leon Schindler[1], and Kristin M. de Payrebrune[1]*

[1] RPTU Kaiserslautern-Landau, Institute for Computational Physics in Engineering, Gottlieb-Daimler-Straße 44, 67663 Kaiserslautern, Germany

Abstract: The key feature of soft robots is the use of soft materials. On the one hand, the softness is advantageous to fulfill tasks for which adaptability is important. On the other hand, the softness is challenging in modeling and design. We are sure that both modeling and design can benefit from sensitivity analysis. To illustrate this, we present two examples of a pneumatic multi-chamber actuator with load. The first example is based on global sensitivity indices and focuses on finding the model parameters of the actuator with the most influence. With this information, the model as well as the design of the actuator can be improved in an iterative process. The second example is based on Monte Carlo filtering and focuses on evaluating the influence of an eccentric external load on the actuator tip position, and the interaction of the parameters characterising the eccentricity position. In this case, the sensitivity analysis improves the general understanding of how external loads influence an actuator.

Keywords: Soft robotics, Sensitivity analysis, Global sensitivity indices, Monte Carlo filtering, Actuator design, Cosserat beam model

1 Introduction

While conventional robots consist of stiff components connected by joints, soft robots are made of soft components. Rus and Tolley (2015) quantify the stiffness of soft robots in a range from 10^4 Pa to 10^9 Pa. Soft materials are advantageous when adaptability is desired to perform a task. For example, the soft STIFF-FLOP manipulator from Cianchetti et al. (2013) is a surgery tool that has a low probability of damaging a patient's internal organs. Another example is a soft robot for the care of elderly people. There are different typical actuation mechanisms in soft robotics, for example pneumatics, tendons or shape memory alloys, as described by Runge et al. (2017). Soft robots using these actuation mechanisms have in common that they are usually underactuated.
Pneumatic multi-chamber bending actuators are a subgroup often used in soft robotics, cf. Suzumori et al. (1991); Trivedi et al. (2007); Cianchetti et al. (2013); Abidi et al. (2017); Toshimitsu et al. (2021). They are based on axially stretching chambers in parallel alignment. The parallel alignment transforms the stretch of the individual chambers into a bending of the actuator. While, for example, Garriga-Casanovas et al. (2018); Fras and Althoefer (2019); Lenssen et al. (2019); Naghibi et al. (2019); Lamping et al. (2022) systematically investigate design aspects of these actuators, trial-and-error seems to be still a common method in soft robotics. However, Garriga-Casanovas et al. (2018) show that useful information regarding the design can be drawn from an analytical model. As in other disciplines, modeling a system always provides the possibility to evaluate the effect of design changes in advance by a simulative testing. The Cosserat beam model is a common model approach for pneumatic multi-chamber bending actuators, cf. Trivedi et al. (2007); Uppalapati et al. (2018); Till et al. (2019); Gilbert and Godage (2019); Bartholdt et al. (2021); Eugster et al. (2022); Lamping and de Payrebrune (2023), where the three-dimensional structure of an actuator is mapped to an one-dimensional curve in space. In order to map the structure of the actuator, assumptions need to be made which differ in each of the studies referred to.
Sensitivity analysis is a generic term for statistical methods which are used to systematically evaluate the influence of input parameters of a model on its output, where local and global sensitivity analysis are usually distinguished. For example, Garcia Morales et al. (2022) use local sensitivity analysis to investigate an origami-based soft actuator. They identify the parameters with the highest influence on the force and contraction of the actuator. The analysis is local since the actuator always remains in an operating point. Bishay and Sofi (2018) use a comparable approach for a soft shape memory alloy driven finger actuator. In contrast, global sensitivity analysis takes not only an operating point and the resulting gradient at this point into account, but a larger range of multiple parameters at once.
To the best of the authors' knowledge, sensitivity analysis has not yet been used in soft robotics, except for the two studies mentioned. In the present study, we aim to illustrate the advantage that global sensitivity analysis provides in soft robotics. For this, we apply a Cosserat beam model of a pneumatic multi-chamber actuator from a preliminary study of Lamping and de Payrebrune (2023) to two loading conditions. The examples are chosen in order to show different methods of sensitivity analysis. In the first example, we calculate sensitivity indices for the parameters of the actuator model, aiming to identify those with the highest influence on the error. In the second example, we evaluate the stability of an actuator for a varying eccentric load by Monte Carlo filtering, aiming to identify the range of loads that can be applied without forcing the tip of the actuator out of a desired spatial range compared to the position without load.

The methods introduced in section 2 comprise an introduction to sensitivity analysis, and the Cosserat beam model of a pneumatic

* E-mail address: kristin.payrebrune@mv.rptu.de
doi: 10.24352/UB.OVGU-2023-063

multi-chamber bending actuator. We use this actuator for the two examples in section 3 and section 4. Finally, we conclude relevant aspects in section 5.

2 Methods

Saltelli et al. (2004) define sensitivity analysis as "the study of how uncertainty in the output of a model (numerical or otherwise) can be apportioned to different sources of uncertainty in the model input". Hence, sensitivity analysis is a generic term that summarizes a variety of (statistical) methods. We restrict the methods in subsection 2.1 to the use cases of this study. However, other methods might also be of interest in soft robotics.
Similar to the sensitivity analysis, the soft actuator and its model in subsection 2.2 are a single example out of various pneumatic multi-chamber actuators and various modeling approaches. We chose this example in order to continue a preliminary study of Lamping and de Payrebrune (2023) where we presented and validated a novel modeling approach based on the Cosserat beam theory. The contribution of the modeling approach is that one-dimensional axial force and stretch measurements of an actuator are sufficient in order to identify the model parameters necessary to simulate its three-dimensional deformation under load. With the sensitivity analysis presented in this study we can subsequently identify the most important parameters to improve accuracy of the model.

2.1 Sensitivity analysis

In the following, we introduce the sensitivity analysis methods used in this study. Saltelli et al. (2004) mention that sensitivity analysis can be subdivided into four settings: Factor Prioritization, Factor Fixing, Variance Cutting and Factor Mapping. An appropriate sensitivity measure depends on the task of the sensitivity analysis and the setting (Saltelli et al. (2007)). For the definition of sensitivity measures in this section, we refer to an input factor of a model as X_i and the corresponding model output $Y = Y(X_1, X_2, \ldots, X_n)$ produced by all input factors n.
As we are interested in identifying input factors with high influence, we make use of the Factor Prioritization setting according to Saltelli et al. (2007) and of the variance-based sensitivity measures called global sensitivity indices S_i and S_{Ti} described by Homma and Saltelli (1996). These sensitivity indices offer the ability to be model independent which means they can operate on non-linear and non-additive models (Homma and Saltelli (1996); Saltelli et al. (2007)). Additionally, they allow the identification of interactions among different input parameters with a total order sensitivity index S_{Ti} (Saltelli et al. (2007)).
Besides the interest in parameters with high influence in general, we are also interested in the Factor Mapping setting, where we use the Monte Carlo filtering method. This method offers the possibility to define a condition for the range of output values and to determine input factor ranges which particularly contribute to a fulfillment of this condition. This is done by mapping the output values back to the corresponding input values, cf. Saltelli et al. (2007).
Conclusions on the sensitivity of the model output to individual input parameters can be drawn by different methods using the different sensitivity settings. We restrict ourselves to the variance-based global sensitivity indices and the Monte Carlo filtering already introduced.

2.1.1 Global sensitivity indices

The brief summary of the variance-based first and total order global sensitivity indices in this subsection is based on Saltelli et al. (2007). The first order sensitivity indices S_i and the total order sensitivity indices S_{Ti} are defined for each input factor X_i. The first order sensitivity indices S_i describe the change on the variance of the output Y by the individual input factors X_i. The total order sensitivity indices S_{Ti} take the interaction effects between an input factor and all other remaining input factors into account.
The first order sensitivity index S_i for an input factor X_i is

$$S_i = \frac{V_{X_i}(E_{X_{-i}}(Y|X_i))}{V(Y)}. \tag{1}$$

The term $V(Y)$ refers to the overall unconditional output variance. $E_{X_{-i}}(Y|X_i)$ is the conditional expected value of the output Y for a fixed value of X_i over all other values except X_i, which is denoted by the subscript X_{-i}. The term $V_{X_i}(E_{X_{-i}}(Y|X_i))$ describes the variance of this conditional expected value over all possible X_i values.
The total order sensitivity index S_{Ti} which, besides the additive part, also includes the interactions with other input factors, is

$$S_{Ti} = 1 - \frac{V_{X_{-i}}(E_{X_i}(Y|X_{-i}))}{V(Y)}. \tag{2}$$

In contrast to the first order sensitivity indices S_i, the conditional expected value of Y is calculated just over X_i by fixing all other input parameters and is denoted by $E_{X_i}(Y|X_{-i})$. The variance $V_{X_{-i}}(E_{X_i}(Y|X_{-i}))$ of this conditional expected value is taken over all input parameters except X_i.
Saltelli et al. (2000) define S_i "as the expected fractional reduction in variance that would be achieved if X_i were known" and S_{Ti} "as the expected fraction of variance that would be left if only X_i were to stay undetermined". We use the extended Fourier Amplitude Sensitivity Analysis (eFAST) introduced by Saltelli et al. (1999) to estimate the sensitivity measures in Equation 1 and Equation 2.

2.1.2 Monte Carlo filtering

The brief summary of the so-called Monte Carlo filtering method in this subsection also refers to Saltelli et al. (2007). Monte Carlo filtering offers the possibility to determine the influence of input parameters based on a threshold value that categorizes the values of the output variable into a "behavioral" B and "non-behavioral" $\overline{B}$ subset. The behavioral and non-behavioral output realizations can be mapped back to the driving input factors, which then can be subdivided into a behavioral subset $(X_i|B)$ and a non-behavioral subset $(X_i|\overline{B})$. After subdivision, one obtains two density functions for each input factor X_i and two associated cumulative distribution functions.
Let $W(X_i|B)$ be the cumulative distribution function of the behavioral subset and, accordingly, $W(X_i|\overline{B})$ of the non-behavioral subset of the input factors X_i. Then the difference between the two cumulative distribution functions can be used as a measure for the influence of the input parameter. The larger the difference, the higher is the influence of an input parameter on the specified threshold condition for the output.
The behavioral subset can be further inspected using a bidimensional projection of this subset into a two dimensional scatter plot of two input parameters. This allows to detect behavioral interactions between two input parameters graphically.

2.2 Actuator model

The actuator under investigation is shown in Figure 1a. Its design results from a systematic investigation of design aspects Lamping et al. (2022) and consists of the following components: three chambers per module in parallel alignment, rings to prevent radial expansion of the chambers, end caps and linking elements to keep the chambers aligned parallel, and a connector for serial stacking. All components except the chambers are 3D printed and rigid (*Visijet M2R*, *3D-Systems GmbH*), but could also be made of silicone preferably stiffer than the chamber. The chambers consist of silicone (*Dragon Skin 10*, *Smooth-On Inc.*). Although individual pressurization of each chamber would be possible, throughout this study stacked chambers are pneumatically connected.
The model of the actuator relates to experiments as shown in Figure 1b. The actuator is clamped in vertical position and deflects due to pressurization with an additionally applied load of 1 N at the free end.

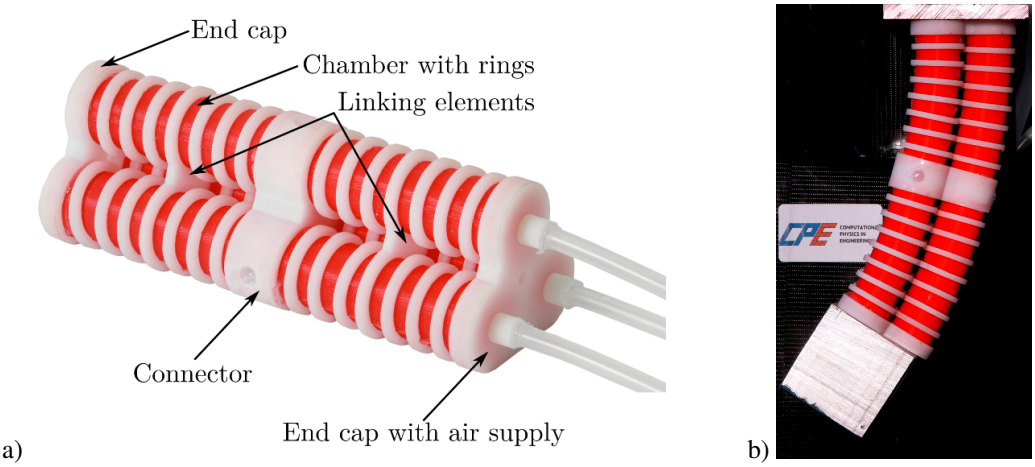

Fig. 1: Three-chamber bending actuator, where stiff components are white and flexible chambers are red a). Experimental setup with the pressurized actuator clamped in vertical position b). Taken from Lamping and de Payrebrune (2023) by CC BY

2.2.1 Cosserat beam model

Beam models, especially the Cosserat beam theory, are a common approach used in soft robotics, cf. Trivedi et al. (2007); Uppalapati et al. (2018); Till et al. (2019); Gilbert and Godage (2019); Bartholdt et al. (2021); Eugster et al. (2022). In contrast to the Euler–Bernoulli beam, the Cosserat beam theory also includes large deformations, axial stretch, twist and shear. This is necessary in order to cover the full range of deformations of soft robots. Transforming the three-dimensional structure of the actuator into a one-dimensional curve in space reduces computational costs. However, since this transformation is a reduction of complexity, accuracy of modeling suffers. The following brief introduction to the Cosserat beam theory is based on Antman (2006) and Cao and Tucker (2008), and is identical to a preliminary study of Lamping and de Payrebrune (2023).
Referring to Figure 2, the beam is represented by its centerline

$$\mathbf{q}(s) = x(s)\mathbf{e}_1 + y(s)\mathbf{e}_2 + (s + z(s))\mathbf{e}_3, \tag{3}$$

where s is the arc-length parameter and $\{\mathbf{e}_1, \mathbf{e}_2, \mathbf{e}_3\}$ is a global coordinate system. The global coordinate system is supplemented by a local coordinate system $\{\mathbf{d}_1, \mathbf{d}_2, \mathbf{d}_3\}$, so-called directors, where $\mathbf{d}_1$ and $\mathbf{d}_2$ are the principal axis of inertia of the beam and

$$\mathbf{d}_3(s) = \mathbf{d}_1(s) \times \mathbf{d}_2(s). \tag{4}$$

An arbitrary vector can be transformed between the two coordinate systems by three successive rotations.

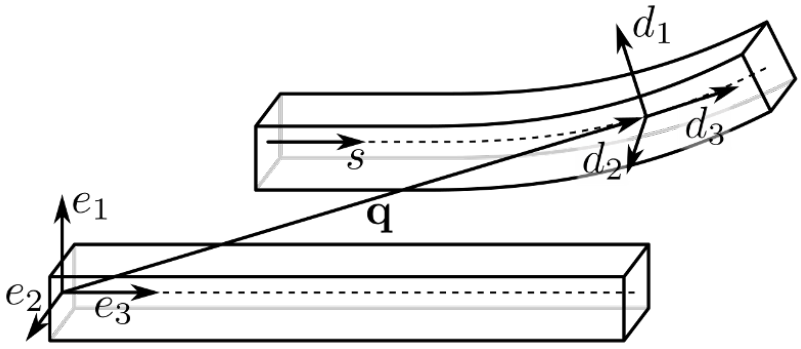

Fig. 2: Coordinate systems of the Cosserat beam. Taken from Lamping and de Payrebrune (2023) by CC BY

The static deformation of the beam results from the equilibrium of forces and moments

$$\mathbf{n}'(s) + \mathbf{f}(s) = \mathbf{0}, \tag{5}$$
$$\mathbf{m}'(s) + \mathbf{q}'(s) \times \mathbf{n}(s) + \mathbf{l}(s) = \mathbf{0}, \tag{6}$$

where $\mathbf{f}$ (force) and $\mathbf{l}$ (moment) are external line loads, $\mathbf{n}$ is the contact force (shear $n_{1/2}$, stretch n_3), and $\mathbf{m}$ is the contact moment (bending $m_{1/2}$, torsion m_3). The superscript $(.)'$ denotes the derivation with respect to the arc-length parameter s.
The magnitude of deformation is measured by $\mathbf{v}$ (shear $v_{1/2}$, axial stretch v_3) and $\mathbf{u}$ (curvature $u_{1/2}$, torsion u_3), where

$$\mathbf{v}(s) = \mathbf{q}(s)', \tag{7}$$
$$\mathbf{d}(s)' = \mathbf{u}(s) \times \mathbf{d}(s). \tag{8}$$

The contact forces and moments result from

$$\mathbf{n} = \mathbf{K}(\mathbf{v} - \mathbf{v}_0), \tag{9}$$
$$\mathbf{m} = \mathbf{J}(\mathbf{u} - \mathbf{u}_0). \tag{10}$$

The subscript $(.)_0$ denotes the initial position of the beam, with $\mathbf{v}_0 = (0, 0, 1)$ and $\mathbf{u}_0 = \mathbf{0}$ representing a straight beam in the $\mathbf{e}_3$-direction. Assuming linear-elastic material behavior,

$$\mathbf{K} = K_{ij}(\mathbf{d}_i \otimes \mathbf{d}_j) \tag{11}$$
$$K_{ij} = \begin{bmatrix} S & 0 & 0 \\ 0 & S & 0 \\ 0 & 0 & E \end{bmatrix},$$

where S is the shear stiffness and E is the extensional stiffness. Analogously,

$$\mathbf{J} = J_{ij}(\mathbf{d}_i \otimes \mathbf{d}_j) \tag{12}$$
$$J_{ij} = \begin{bmatrix} G & 0 & 0 \\ 0 & G & 0 \\ 0 & 0 & T \end{bmatrix},$$

where G is the bending stiffness and T is the torsional stiffness. For ease of reading, the stiffnesses S, E, G and T are combined quantities, which comprise material stiffness as well as geometrical aspects, e.g. the extensional stiffness E for linear elasticity (unit N) is defined as the product of the Young's modulus and the cross sectional area and the bending stiffness G (unit Nm^2) is defined as the product of Young's modulus and second moment of inertia. Similar to others, as Trivedi et al. (2007); Uppalapati et al. (2018); Till et al. (2019); Gilbert and Godage (2019); Uppalapati and Krishnan (2020), we restrict the model to the extensional stiffness E and the bending stiffness G when performing simulations in this study. The shear stiffness S and the torsional stiffness T are considered infinite.
An important aspect being related to pneumatic soft robots is to consider pressurization in the beam model. One opportunity is to assume an initial deformation induced by pressure as in Uppalapati et al. (2018); Gilbert and Godage (2019). Another opportunity used by Trivedi et al. (2007); Hadi Sadati et al. (2017); Till et al. (2019); Bartholdt et al. (2021); Eugster et al. (2022), and also chosen in this study, is to modify the equilibrium of forces and moments

$$(\mathbf{n} - \mathbf{F})'(s) + \mathbf{f}(s) = \mathbf{0} \tag{13}$$
$$\mathbf{m}'(s) + \mathbf{q}'(s) \times \mathbf{n}(s) + \mathbf{M}'(s) + \mathbf{q}'(s) \times \mathbf{F}(s) + \mathbf{l}(s) = \mathbf{0}, \tag{14}$$

and to apply counteracting jumping conditions for $\mathbf{F}$ and $\mathbf{M}$ at the ends of a pressurized section. Here, $\mathbf{F} = F\mathbf{d}_3$ is the axial force induced by pressure and $\mathbf{M} = M_1\mathbf{d}_1 + M_2\mathbf{d}_2$ are the corresponding moments.

2.2.2 Model preparation for sensitivity analysis

To simulate the experimental setup in Figure 1b, we implemented the Cosserat beam as a boundary value problem in *Matlab R2021b* using the *bvp4c* solver. According to Figure 3 and Table 1, we axially divide the beam in five regions because the actuator under investigation consists of multiple components of different weight and length. The weight attached to the free end of the actuator is considered as additional point load (force and moment) at the end of the beam. All components except the chambers are rigid. Thus, we consider infinite extensional stiffness E and bending stiffness G for regions 1, 3, and 5.

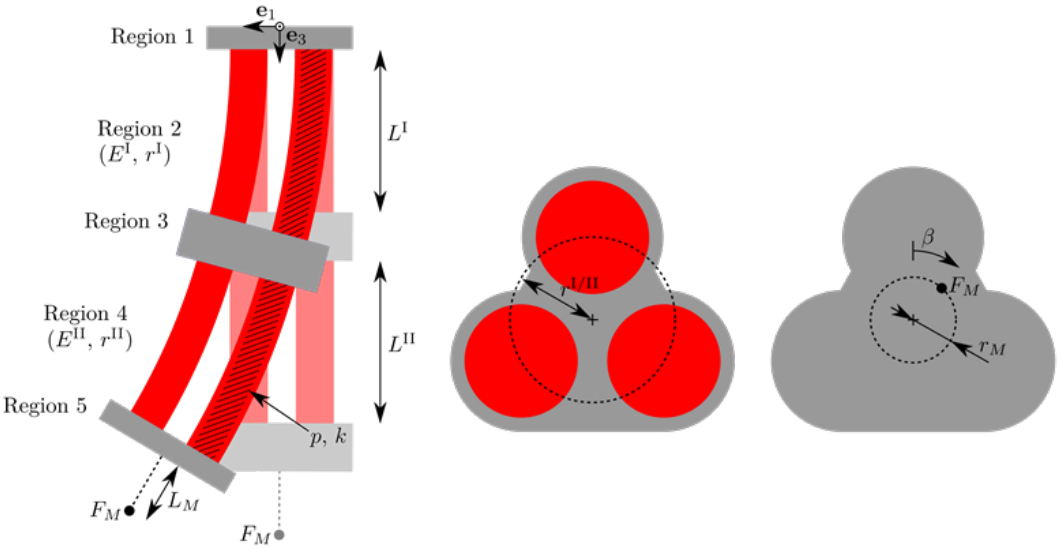

Fig. 3: Schematic of the experimental setup with parameters used in the simulation

Tab. 1: Weight and length of regions used in the simulation, from fixed end to free end

Region	Components of real actuator	Weight in kg	Length in m
1	Fixed end cap	$4.0 \cdot 10^{-3}$	$3.5 \cdot 10^{-3}$
2	Chambers + rings	$25.0 \cdot 10^{-3}$	$44.8 \cdot 10^{-3}$
3	Connector cap	$8.3 \cdot 10^{-3}$	$9.0 \cdot 10^{-3}$
4	Chambers + rings	$25.0 \cdot 10^{-3}$	$44.8 \cdot 10^{-3}$
5	Free end cap	$4.0 \cdot 10^{-3}$	$3.5 \cdot 10^{-3}$

In addition to the weight and length, four groups of parameters need to be known in order to simulate a pneumatic soft actuator as a Cosserat beam: 1. the dimensions of the actuator, 2. the stiffness of the material, 3. the effect of pressurization, and 4. external loads. Table 2 and Table 3 list all parameters we vary for the beam parameter analysis in section 3 and the stability analysis in section 4, respectively. All parameters are uniform distributed in the specified range. The superscript $(.)^{\mathrm{I/II}}$ denotes that a quantity is individually varied for the chambers in region 2 and region 4 of the actuator.
In the following, we discuss the individual parameters of the four groups. If no other explanation is given, the assumptions chosen are based on a preliminary study of Lamping and de Payrebrune (2023). However, since the presented sensitivity analysis is independent from the preliminary study, the parameters only need to be consistent relative to each other in order to create a realistic example.

Tab. 2: Beam parameters varied for the beam parameter analysis (section 3)

Parameter		Ideal	Range
$L^{\mathrm{I/II}}$	Length of chambers in m	44.8×10^{-3}	$\pm 0.2 \times 10^{-3}$
$r^{\mathrm{I/II}}$	Radius of chamber arrangement in m	11.55×10^{-3}	$\pm 0.5 \times 10^{-3}$
$E^{\mathrm{I/II}}$	Extensional stiffness in N	200	± 20
p	Air pressure in kPa	90	± 1
k	Scaling factor of cross section area in kPa^{-1}	5.3×10^{-3}	$\pm 1 \times 10^{-3}$
M	External load in N	1	± 0.02
L_M	Distance of the external load to the actuator tip in m	17.5×10^{-3}	$\pm 1 \times 10^{-3}$
r_M	Eccentricity radius of the load in m	0	1×10^{-3}
β	Eccentricity angle of the load in °	-	0 to 360

Tab. 3: Beam parameters varied for the stability analysis (section 4)

Parameter		Ideal	Range
M	External load in N	0	2.5
L_M	Distance of the external load to the end cap in m	-	0 to 50×10^{-3}
r_M	Distance of the external load to the centerline m	-	0 to 10×10^{-3}
β	Angular position of the external load in °	-	0 to 360

Dimensions of the actuator While other quantities, such as the stiffness of the material, need to be determined experimentally, the dimensions of the actuator are known. However, due to hand manufacturing, little deviations between planned design and real actuator might occur.
From the variety of dimensions, we vary the length of the chambers $L^{\mathrm{I/II}}$ and the radius of the chamber arrangement $r^{\mathrm{I/II}}$ in a small range. As shown in the next paragraph, the radius $r^{\mathrm{I/II}}$ has an influence on the bending stiffness. $L^{\mathrm{I/II}}$ as well as $r^{\mathrm{I/II}}$ have a direct influence in the model. Other dimensions are considered implicitly. For example, the inner and outer radius of the chambers influence the extensional stiffness $E^{\mathrm{I/II}}$ which is a combined quantity of cross section and material stiffness, and a varying distance between rings influences the scaling factor k of the cross section area for ballooning introduced later.

Stiffness of the material The extensional stiffness $E^{\mathrm{I/II}}$ and the bending stiffness $G^{\mathrm{I/II}}$ fully define the stiffness of the material, since the shear stiffness and torsional stiffness are considered infinite. In the preliminary study, we experimentally identified $E = 180\,\mathrm{N}$ to $220\,\mathrm{N}$, and, for practical reasons, used the mean value $E = 200\,\mathrm{N}$. However, for the sensitivity analysis, we use the experimentally identified range. We assume that the bending stiffness is

$$G^{\mathrm{I/II}} = \frac{E^{\mathrm{I/II}}}{2} \cdot (r^{\mathrm{I/II}})^2 \cdot v_3, \tag{15}$$

where v_3 is the axial stretch from Equation 7. Hence, in the sensitivity analysis the bending stiffness is implicitly varied by the variation of the extensional stiffness $E^{\mathrm{I/II}}$ and the radius $r^{\mathrm{I/II}}$.

Effect of pressurization The quality of the pressure control directly influences the effect of pressurization. We assume that an industrial pressure controller is able to control a pressure of 90 kPa with an uncertainty of 1 kPa.
In order to determine the axial force F induced by pressure p, we use an experimentally identified cross section area $A = 76{\times}10^{-6}\,\mathrm{m}^2$. Since the chambers of the actuator balloon between rings, we also consider a scaling factor k for the cross section area such that

$$F_j = A \cdot (1 + k p_j) \cdot p_j, \tag{16}$$

$$F = \sum_{j=1}^{3} F_j, \tag{17}$$

where the subscript $(.)_j$ distinguishes between the individual chambers of the actuator. Eugster et al. (2022) use a similar factor which scales the radius instead of the cross section area. Note that we assume pressurization of only a single chamber as shown in Figure 3.
The moment induced by pressure results from the axial forces F_j of the individual chamber and the radius of the chamber arrangement $r^{\mathrm{I/II}}$. Hence, the moment is implicitly varied by the pressure p, the scaling factor k and the radius $r^{\mathrm{I/II}}$.

External loads From the model perspective, the self-weight of the actuator is a load similar to other external loads. Referring to Table 1, we assume that the weight and length of the individual components are known. We vary only the length of the chambers $L^{\mathrm{I/II}}$ in the sensitivity analysis while keeping their self-weight at a fixed value.
In the real experiment shown in Figure 1b, a weight is attached to the free end of the actuator. Referring to Figure 3, we assume that this weight is a point load M with a distance L_M to the end cap that induces a force and a moment at the end of the actuator. However, the point load is eccentric, which means it is not on the extension of the centerline of the actuator. We use polar coordinates r_M and β to define the position of the point load relative to the centerline in the local $\mathbf{d}_1$-$\mathbf{d}_2$-plane. Note that, due to the polar coordinates, a uniform distribution of r_M and β leads to a non-uniform sample density of weight positions with a higher density close to the centerline of the actuator.

Model ouput The aim of sensitivity analysis is to study the influence of the described model parameters on an output. In our case, the output is the euclidean distance ΔR of the sampled actuator tip positions to a nominal position. The nominal position is the position for "ideal parameters" as shown in Table 2 and Table 3. We thus assume that the real actuator is described exactly by the ideal parameters and evaluate the influence if those parameters are not identified correctly experimentally or if the external load at the actuator tip changes.
For the Monte Carlo filtering, the sample tip positions need to be subdivided in a behavioral group and a non-behavioral group. We perform the subdivision by defining an accepted euclidean distance ΔR between sample tip positions and nominal position.

3 Beam parameter analysis

The first example of the application of sensitivity analysis in soft robotics is a critical evaluation of beam model parameters. We start from the hypothesis that the "ideal" parameters in Table 2 are the exact parameters of a real actuator and that the "range" represents the uncertainties of an experimental parameter investigation.

3.1 Effect of single parameter changes

To visualize the effect of a parameter change on the elongated soft robot a local approach is used first. In this approach the parameters pressure p and external load M are varied within their respective ranges and all other parameters are set to the "ideal" values. Figure 4a shows the elongated soft robot modeled as a beam through its centerline. The effect from the variation of the external load M is not directly visible on the macroscopic level. To illustrate the change in the tip position of the soft robot, a detailed view is shown in Figure 4b. Only the displacements in $\mathbf{e}_1$- and $\mathbf{e}_3$-direction are shown because the bending of the soft robot only occurs in the $\mathbf{e}_1$-$\mathbf{e}_3$-plane. As the changes are minor compared to the size of the soft robot we focused on the change of tip position. If the pressure p is increased, the displacement in $\mathbf{e}_1$-direction increases, whereas if the external load M increases the displacement in $\mathbf{e}_1$-direction decreases. The tip positions have been projected in the $\mathbf{e}_1$-M-plane and the projected points with equal pressure have been connected by a line.

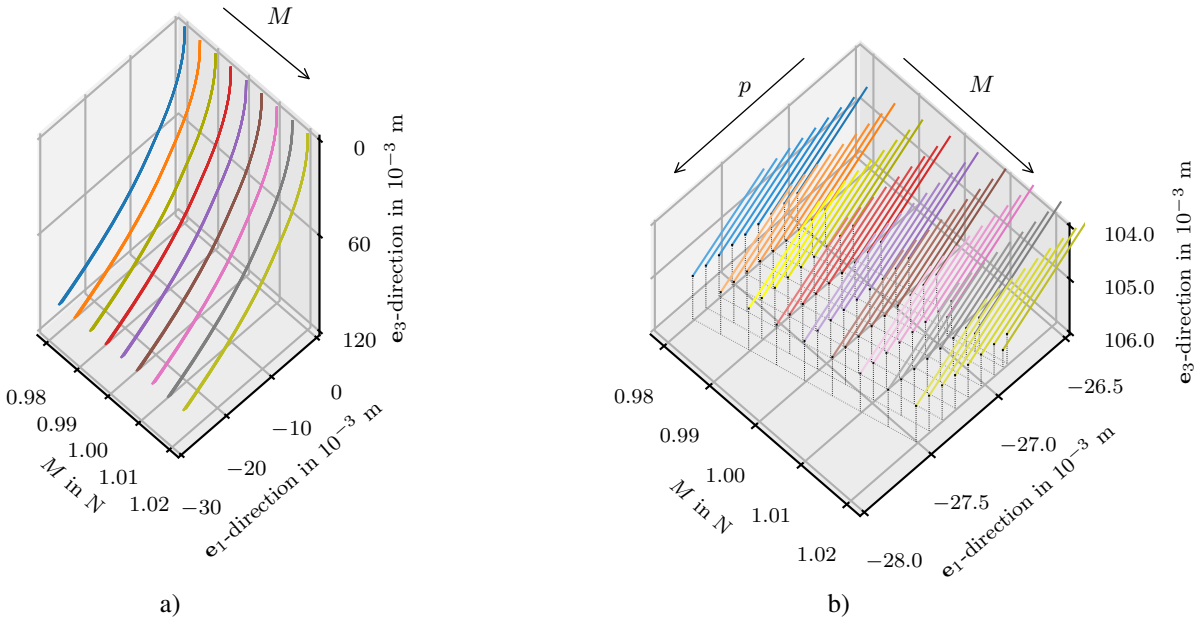

Fig. 4: Beam curvature of the simulated soft robot when changing pressure p and external load M for the complete beam a), and detailed view at the tip position b)

3.2 Spatial distribution

The first step of a sensitivity analysis is to create sample points from the parameters and their range, and to perform simulations with these samples. Figure 5 shows the scatter of the spatial sample distribution in the $\mathbf{e}_1$-$\mathbf{e}_3$-plane, each with a color bar for the length L^{I} of Region 2, the pressure p, and the scaling factor k. The $\mathbf{e}_1$-$\mathbf{e}_2$-plane and the $\mathbf{e}_2$-$\mathbf{e}_3$-plane are not shown since the deviations in these planes are little. In order to demonstrate that some conclusions can be drawn even without the statistic methods of the sensitivity analysis, we chose these three parameters as an example.

The gradient of colors in Figure 5a clearly indicates a dependency of the sample points on the length L^{I} of Region 2. However, the gradient is roughly along the $\mathbf{e}_3$-direction, while the main spread of the sample point distribution is in $\mathbf{e}_1$-direction. Thus, the influence of the uncertainty of L^{I} is little.

The influence of the pressure p in Figure 5b is also little since the sample points are randomly distributed and no gradient is visible.

In contrast, a significant influence of the scaling factor k results from Figure 5c. The gradient of colors is roughly along the $\mathbf{e}_1$-direction, in which the sample point distribution also mainly spreads.

3.3 Sensitivity indices

The sensitivity indices in Figure 6 result from the distribution of sample points in Figure 5. Note that we increased the number of sample points when determining the sensitivity indices.

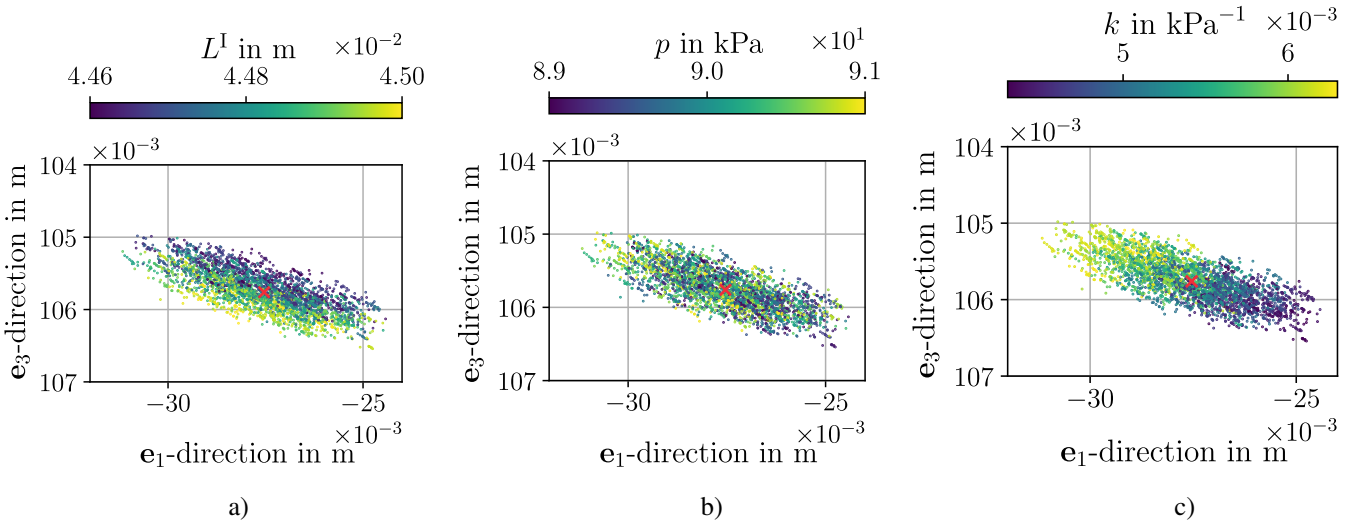

Fig. 5: Scatter plots of output uncertainty with ideal positions marked by a red cross and color mapping for the input parameters length L^{I} of Region 2 a), pressure p b) and scaling factor k c)

Regarding the first order sensitivity indices S_i, only the extensional stiffness E^{I} of Region 2 and the scaling factor k have noticeable influence. The influence of E^{I} is higher than that of E^{II} since Region 2 is at the base of the actuator which increases the leverage. The total sensitivity indices S_{Ti} also take the interaction of the beam parameters into account. With this measure, the extensional stiffness E^{II} of Region 4, the radius of the chamber arrangement r^{I} of Region 2, and the pressure p also have a noticeable influence. However, the influence of the extensional stiffness E^{I} of Region 2 and the scaling factor k are still most significant.

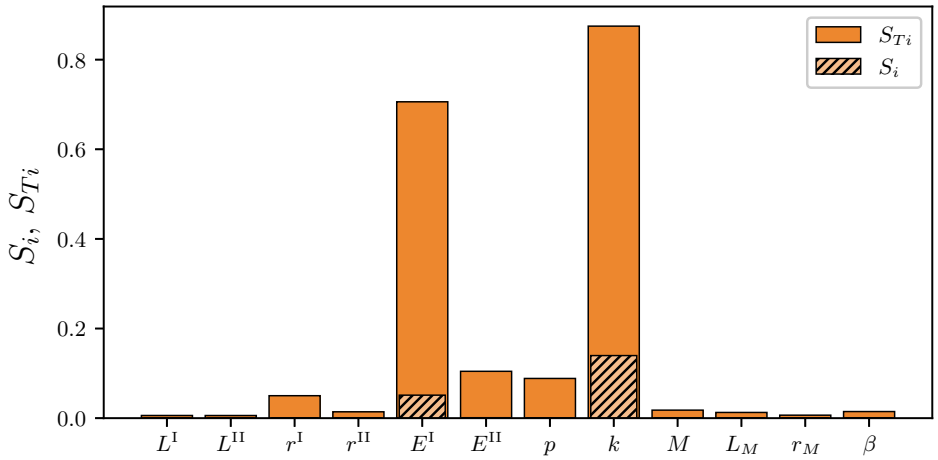

Fig. 6: First sensitivity indices S_i and total order global sensitivity indices S_{Ti} for each parameter of Table 2

3.4 Discussion of beam parameters

Some relevant conclusions to improve model accuracy can be drawn from the sensitivity indices. Naturally, a more refined experimental parameter identification itself leads to higher accuracy. However, we restrict to conclusions beyond improving experiments.

Scaling factor k The scaling factor k represents ballooning of the actuator chambers at higher pressure. The higher the pressure is, the more influence has k. For the actuator under investigation, ballooning is likely to occur due to the large distance between the reinforcing rings. The high significance of uncertainties of the scaling factor k depicts the relevance of ballooning. This can be anticipated in two ways in order to model an actuator accurately.

On the one hand, the model itself could be improved, since the scaling factor is only a rough approximation of the effect of ballooning. This would also reduce the uncertainty of the parameter identification since the parameters of such an improved model have a physical counterpart. For example, in a preliminary study of Lamping and de Payrebrune (2021), we propose a model for individual pneumatic cylinders which takes ballooning into account.

On the other hand, the design is relevant for the intensity of ballooning and could be adapted. For example, the wall thickness and the distance between rings influence ballooning, as shown in a preliminary study (Lamping et al. (2022)). Thicker walls would reduce the effect of a varying distance between rings due to manufacturing errors. The distance between rings or fibers, respectively, should be as regular as possible.

Extensional stiffness E As already mentioned, the uncertainty of the extensional stiffness E^{I} of Region 2 has a higher influence on the model output than the uncertainty of the extensional stiffness E^{II} of Region 4 due to leverage. However, it can be assumed that in reality both are not determined individually. Remember that the extensional stiffness E combines the stiffness of the material as well as its cross section. Hence, both aspects are relevant to reduce the uncertainty of the extensional stiffness E.
The stiffness of the material depends on the manufacturing process. Case et al. (2015) state that the properties of two samples of silicone typically used in soft robotics are never the same unless they are from the same charge. Nevertheless, the deviations can be reduced through careful manufacturing. One reason for deviations is a varying amount of air bubbles in every charge (Schmitt et al. (2018)), another reason is the mix ratio of the silicone components which might differ (Schmitt et al. (2018); Case et al. (2015)). Experience shows that the curing temperature also has an influence. However, to the best of the authors' knowledge, there has been no systemic study of this aspect yet.
The cross section of the material can deviate through tolerances of the casting process. Assuming that the absolute tolerance of casting is constant, the relative error of the tolerances increases for thinner walls. Therefore, any tapering of the actuator wall should be prevented.

Pressure p Although the uncertainty of the pressure p has the third highest influence on the model output, the influence of the scaling factor k and of the extensional stiffness E is significantly higher. We assume that the error of the pressure control is constant, i.e. the relative error is larger for lower pressure and the influence on the model output increases.

Dimensions The uncertainty of the length of the chambers $L^{\mathrm{I/II}}$ and of the radius of the chamber arrangement $r^{\mathrm{I/II}}$ have little influence on the model output. Deviations of $L^{\mathrm{I/II}}$ can occur since the chambers are cut to the correct length after casting, the deviations of $r^{\mathrm{I/II}}$ result from 3D-printing.

External load We assume that the load in an experimental setup is well known. In the setup in Figure 1b, the external load is an aluminum cube. In this case, the hrough-hole required to attach the cube to the actuator might not be perfectly centered. Nevertheless, for the assumptions chosen, the influence of the uncertainty of the external load is little.

Influence of assumptions The conclusions just discussed refer to the individual scenario in Table 2. We point out that the results of a sensitivity analysis strongly depend on the underlying assumptions. This is important since the uncertainty of some parameters can only be estimated. For example, the scaling factor k has no physical counterpart, which makes an estimation challenging. Halving k from $\pm 1 \times 10^{-3}\,\mathrm{Pa}^{-1}$ to $\pm 0.5 \times 10^{-3}\,\mathrm{Pa}^{-1}$, the influence of the extensional stiffness E^{I} becomes higher than of the scaling factor k. Consequently, the assumptions of a sensitivity analysis should be chosen carefully.
From another perspective, the sensitivity analysis can be seen as a part of the design and modeling process. First, those parameters with the highest influence, based on the current assumptions, are identified. Second, the model or the design are adapted and the assumptions of the sensitivity analysis updated. With this procedure, an optimal solution for a simple, but detailed model, and a design with little influence of manufacturing errors can be found.

4 Stability analysis

The second example of the application of sensitivity analysis in soft robotics is a stability analysis. We start from the hypothesis that the loads acting on a soft robot in a real application can deviate from the loads assumed in the design process, but should thereby influence the deformation behavior as little as possible. Sensitivity analysis is a useful tool for identifying load limits at which the deformations of a soft robot are most likely to remain within a desired range, and for better understanding the interrelationship between the parameters external load M, distance L_M between the external load and the actuator tip, eccentricity radius r_M, and eccentricity angle β.

4.1 Output distribution

The output distribution of the samples of the sensitivity analysis in Figure 7 is a possibility for an analysis without statistical tools, similar to the spatial distribution in Figure 5. An output distribution shows the scatter of the sample points relative to one parameter. For example, in Figure 7a, the euclidean distance ΔR of all samples depending on the mass is given. Conclusions can be drawn from the distribution of the samples.
The sample output distribution relative to the external load M in Figure 7a has little spread compared to the other parameters in Figure 7b-d. This implies that the influence of the external load M on the model output ΔR dominates the influence of the other parameters. Consequently, the limit of the load that should be applied to the actuator is mostly determined by the external load M, while the eccentricity can vary in the range assumed. However, some conclusions can also be drawn from the output distribution of the other parameters.
The expected value of the distance L_M between the external load and the actuator tip slightly slopes in Figure 7b. The slope indicates lower deviations of the actuator tip with load compared to a tip without load if the load is close to the actuator tip.
We assume that a load is always preferred to be applied centered. Although the range of the eccentricity radius r_M in Table 3 is relatively large, the expected value of the output does not change noticeable. Only the maximums of ΔR indicate that the eccentricity radius r_M has any influence.

In contrast, the expected value slightly depends on the eccentricity angle β_M. This is the case because the angle has an influence on the leverage when the actuator is in a bent position, as in the experimental setup chosen. However, the angle with the lowest spread depends on the direction of bending.

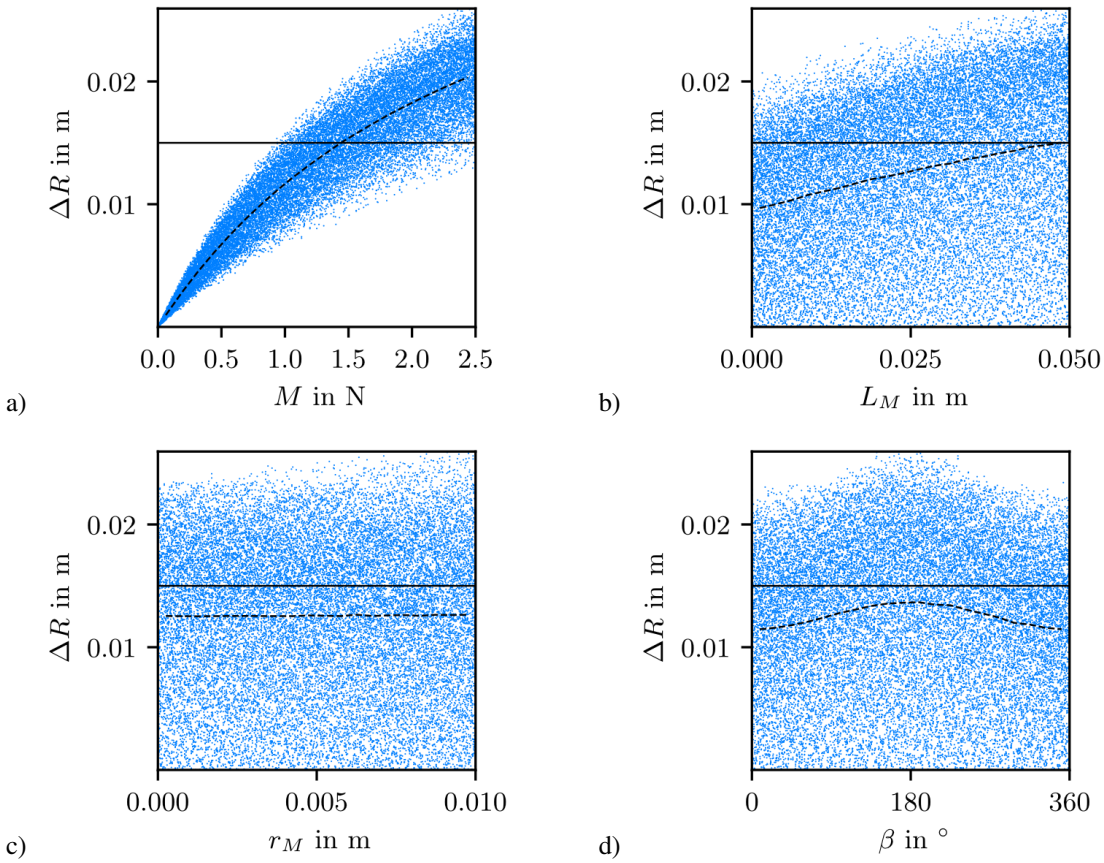

Fig. 7: Distribution of euclidean distance ΔR from sample position to nominal position, conditional expected value (dashed) and threshold value (solid) for external load M a), load distance L_M b), eccentricity radius r_M c) and eccentricity angle β d).

4.2 Cumulative distribution functions

We use a threshold of $\Delta R = 15 \times 10^{-3}$ m to subdivide the samples into "behavioral" and "non-behavioral". Figure 8 shows the resulting cumulative distribution functions of both groups. Remember that the maximum of the difference of both distribution functions measures the influence of a parameter on the output. The higher the maximum difference, the more important is the parameter. In the following, we interpret the course of the cumulative distribution functions in Figure 8.
Figure 8a has the highest maximum difference between the cumulative distribution functions which indicates a significant influence of the external load M. The slope of the behavioral curve is high for little loads, i.e. little loads increase the chance that the actuator tip remains in the desired range.
According to the maximum difference of the cumulative distribution functions, the influence of the distance L_M between the external load and the actuator tip on the model output in Figure 8b is the second highest. Again, the slope of the behavioral curve is higher for smaller L_M, i.e. L_M should be chosen as small as possible.
The difference of the cumulative distribution functions of the eccentricity radius r_M is approximately zero, indicating no influence of this parameter. The difference for the eccentricity angle β_M is little, where the slope indicates the angle should be chosen close to 0° or 360°, respectively. This angle is due to the experimental setup and would differ for bending in another direction.

4.3 Bidimensional projections

Bidimensional projections as shown in Figure 9 are a possibility for a graphical analysis of the interaction of parameters after subdividing them into behavioral and non-behavioral groups. In these projections, only the samples of the behavioral group are plotted with two parameters as axis. Since the external load M has the highest influence, we only discuss the interaction of M with the other parameters.
The scatter of the samples in Figure 9a suggests that external loads M and distance L_M of the external load to the actuator tip are inversely proportional to each other. The lower the distance L_M is, the higher the load M can be chosen. This is in accordance with reality, where the moment applied to the actuator tip is the product of L_M and M.
In contrast, the interrelation of the load M and the eccentricity radius r_M in Figure 9b is less pronounced but proportional, i.e. a higher load can be applied for a larger radius. This contraintuitive behavior is due to the experimental setup, where an eccentricity can reduce the leverage of the external load.

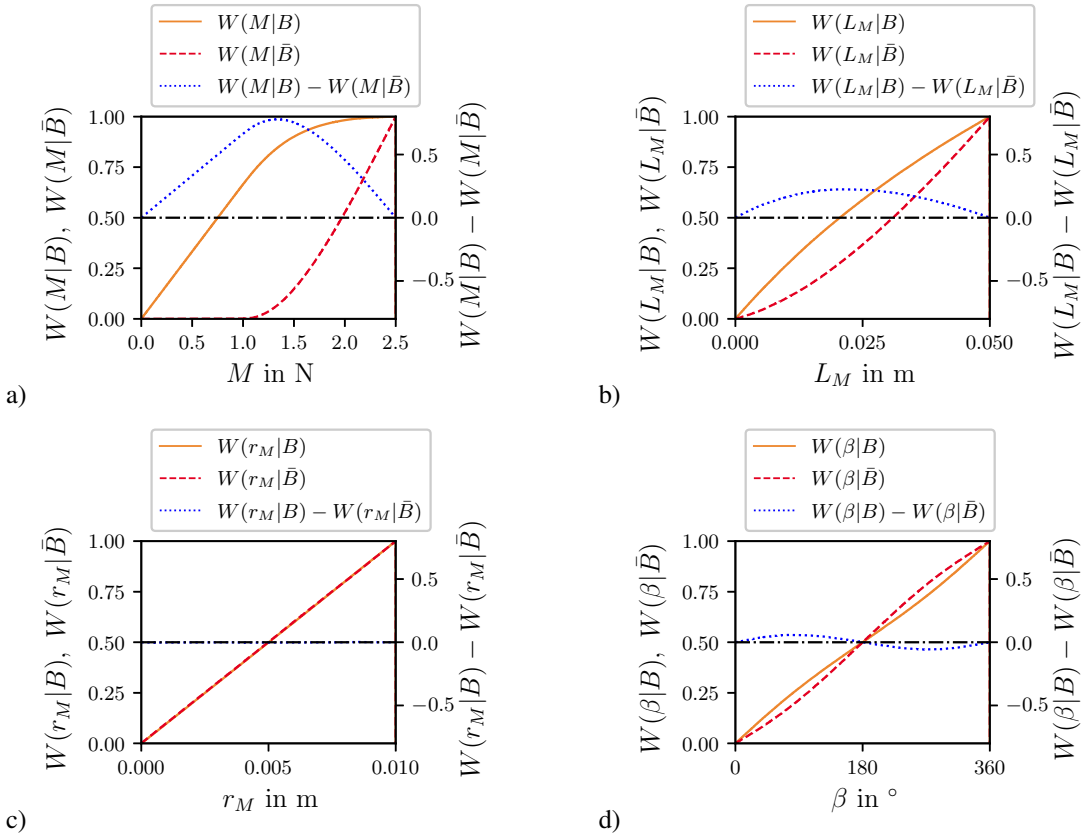

Fig. 8: Cumulative distribution functions W for behavioral and non-behavioral subset of the external load M a), the load distance L_M, b) the eccentricity radius r_M c) and the eccentricity angle β_M d).

As already mentioned, eccentricity angles β_M close to 0° and 360°, respectively, allow higher external loads due to the direction of bending in the experimental setup. The scatter of samples in Figure 9c also indicates this fact. Neither a proportional nor an inversely proportional relation can be identified.

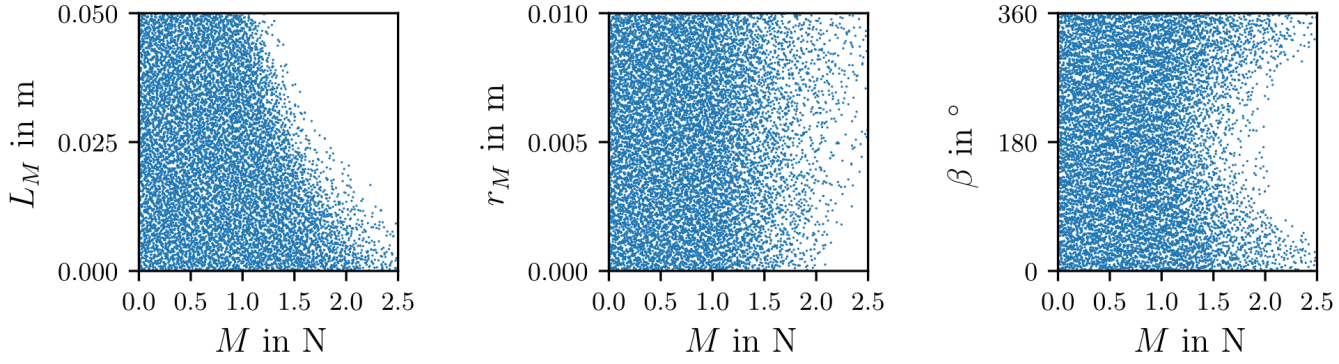

Fig. 9: Bidimensional projections of samples of M in the behavioral subset in combination with the load distance L_M a), the eccentricity radius r_M b) and the eccentricity angle β_M c)

4.4 Discussion of stability analysis

We chose the example of stability analysis in order to illustrate Monte Carlo filtering. The external load M is the parameter with the highest influence on the model output, which becomes clear both from the output distribution and the cumulative distribution functions.

With this previous knowledge, it is reasonable to investigate the interaction of the load M with the other parameters by bidimensional projections. While the importancy of M could also have been identified by the same sensitivity indices as in section 3, the interaction is a useful additional information. For example, the interaction with the eccentricity angle β_M points out that the eccentricity in the example is not only a disadvantage, but can be used to lower the influence of the load.

5 Conclusion

The aim of this study is to illustrate the advantage that sensitivity analysis provides in soft robotics. Specified discussions and remarks regarding the two examples can be found in section 3 and section 4. In the following, we conclude sensitivity analysis in soft robotics on a more general level.
The sensitivity indices in section 3 quantify the influence of uncertainties of individual beam parameters on the model output. With this knowledge, the model as well as the underlying design can be optimized in an iterative process. For example, irrelevant parameters provide a possibility to reduce the complexity of the model while relevant parameters provide the possibility to appositely modify the model. In a similar fashion, the relevant parameters suggest changes of the design. After adaptions, another sensitivity analysis is the basis for the next iteration. In the long-term, the accuracy of the model improves while the computational costs reduce. This is beneficial for all areas of soft robotics where models are applied, for example control or path planning.
Monte Carlo filtering allows to deduce the interaction of parameters such that a desired behavior is maintained within a defined range. The threshold condition or the threshold value for the Monte Carlo filtering can be chosen with an application specific strictness. A lower threshold value should be used where accuracy is necessary. The interaction of parameters is an important general information for better understanding an actuator and its model. For example, section 4 shows that the deviation of the actuator tip can decrease for a certain eccentricity angle β_M. Hence, external loads can be applied in a fashion which reduces the influence on the actuator. A better understanding of the actuator also allows to define use cases with high informative value. This could be used to develop specified tests in order to compare different actuators.
Using a different assumption in order to investigate the elongation of the soft robot, the interaction of the load parameters could vary. This is due to the way how the eccentric load acts on the tip of the soft robot. Considering a straight elongation of the soft robot the influence of the eccentric radius r_M might be much higher than the influence of the distance L_M, depending on the assumed uncertainties. Therefore it might be beneficial to set up not just one orientation and actuation of the soft robot, but a set of different spatial arrangements with different actuations to classify the influence of parameters for each of these.
From the authors' perspective, the examples presented in this study illustrate the advantage of sensitivity analysis in soft robotics. However, the bandwidth of applications is large and depends on the type of actuator and the information that should be extracted from the sensitivity analysis. Hence, further research should be made in future.

Acknowledgments

Funded by the Deutsche Forschungsgemeinschaft (DFG, German Research Foundation) – 501861263 – SPP2353 and 404986830 – SPP2100

References

H. Abidi, G. Gerboni, M. Brancadoro, J. Fras, A. Diodato, M. Cianchetti, H. Wurdemann, K. Althoefer, and A. Menciassi. Highly dexterous 2-module soft robot for intra-organ navigation in minimally invasive surgery. *The International Journal of Medical Robotics and Computer Assisted Surgery*, 14(1):e1875, dec 2017. doi: 10.1002/rcs.1875.

S. S. Antman. *Nonlinear Problems of Elasticity*. Springer New York, 2006. URL http://www.ebook.de/de/product/11430282/s_s_antman_stuart_s_antman_nonlinear_problems_of_elasticity.html.

M. Bartholdt, M. Wiese, M. Schappler, S. Spindeldreier, and A. Raatz. A parameter identification method for static cosserat rod models: Application to soft material actuators with exteroceptive sensors. In *2021 IEEE/RSJ International Conference on Intelligent Robots and Systems (IROS)*, pages 624–631. IEEE, sep 2021. doi: 10.1109/iros51168.2021.9636447.

P. L. Bishay and A. R. Sofi. Sensitivity analysis of a smart soft composite robotic finger design using geometrically nonlinear laminated composite finite beam elements. *Materials Today Communications*, 16:111–118, 2018.

D. Q. Cao and R. W. Tucker. Nonlinear dynamics of elastic rods using the cosserat theory: Modelling and simulation. *International Journal of Solids and Structures*, 45(2):460 – 477, 2008. doi: https://doi.org/10.1016/j.ijsolstr.2007.08.016.

J. C. Case, E. L. White, and R. K. Kramer. Soft material characterization for robotic applications. *Soft Robotics*, 2(2):80–87, jun 2015. doi: 10.1089/soro.2015.0002.

M. Cianchetti, T. Ranzani, G. Gerboni, I. De Falco, C. Laschi, and A. Menciassi. Stiff-flop surgical manipulator: Mechanical design and experimental characterization of the single module. In *2013 IEEE/RSJ International Conference on Intelligent Robots and Systems (IROS)*, pages 3576–3581. IEEE, 2013. doi: 10.1109/IROS.2013.6696866.

S. R. Eugster, J. Harsch, M. Bartholdt, M. Herrmann, M. Wiese, and G. Capobianco. Soft pneumatic actuator model based on a pressure-dependent spatial nonlinear rod theory. *IEEE Robotics and Automation Letters*, 7(2):2471–2478, apr 2022. doi: 10.1109/lra.2022.3144788.

J. Fras and K. Althoefer. Soft fiber-reinforced pneumatic actuator design and fabrication: Towards robust, soft robotic systems. In *Towards Autonomous Robotic Systems*, pages 103–114. Springer International Publishing, 2019. doi: 10.1007/978-3-030-23807-0_9.

D. S. Garcia Morales, C. Jiang, and A. Raatz. Sensitivity analysis for 3d printed soft pneumatic actuators from 2d origami patterns to functional systems. In *2022 IEEE 5th International Conference on Soft Robotics (RoboSoft)*. IEEE, 2022. doi: 10.1109/robosoft54090.2022.9762110.

A. Garriga-Casanovas, I. Collison, and F. Rodriguez y Baena. Toward a common framework for the design of soft robotic manipulators with fluidic actuation. *Soft Robotics*, 5(5):622–649, oct 2018. doi: 10.1089/soro.2017.0105.

H. B. Gilbert and I. S. Godage. Validation of an extensible rod model for soft continuum manipulators. In *2019 2nd IEEE International Conference on Soft Robotics (RoboSoft)*. IEEE, apr 2019. doi: 10.1109/robosoft.2019.8722721.

S. M. Hadi Sadati, S. E. Naghibi, A. Shiva, Y. Noh, A. Gupta, I. D. Walker, K. Althoefer, and T. Nanayakkara. A geometry deformation model for braided continuum manipulators. *Frontiers in Robotics and AI*, 4(22), jun 2017. doi: 10.3389/frobt.2017.00022.

T. Homma and A. Saltelli. Importance measures in global sensitivity analysis of nonlinear models. *Reliability Engineering & System Safety*, 52(1):1–17, 1996. ISSN 0951-8320. doi: 10.1016/0951-8320(96)00002-6.

F. Lamping and K. M. de Payrebrune. A virtual work model for the design and parameter identification of cylindrical pressure-driven soft actuators. *Journal of Mechanisms and Robotics*, 14(3), nov 2021. doi: 10.1115/1.4052849.

F. Lamping and K. M. de Payrebrune. A novel and practicable approach for determining the beam parameters of soft pneumatic multi-chamber bending actuators. *Applied Sciences*, 13(5):2822, 2023.

F. Lamping, D. Müller, and K. M. de Payrebrune. A systematically derived design for a modular pneumatic soft bending actuator. In *2022 IEEE 5th International Conference on Soft Robotics (RoboSoft)*. IEEE, apr 2022. doi: 10.1109/robosoft54090.2022.9762087.

J. A. Lenssen, H. Naghibi, and M. Abayazid. Evaluation of design aspects of modular pneumatic soft robotic endoscopes. In *2019 2nd IEEE International Conference on Soft Robotics (RoboSoft)*. IEEE, apr 2019. doi: 10.1109/robosoft.2019.8722749.

H. Naghibi, M. W. Gifari, W. Hoitzing, J. W. Lageveen, D. M. M. van As, S. Stramigioli, and M. Abayazid. Development of a multi-level stiffness soft robotic module with force haptic feedback for endoscopic applications. In *2019 International Conference on Robotics and Automation (ICRA)*. IEEE, may 2019. doi: 10.1109/icra.2019.8793584.

G. Runge, M. Wiese, and A. Raatz. FEM-based training of artificial neural networks for modular soft robots. In *2017 IEEE International Conference on Robotics and Biomimetics (ROBIO)*. IEEE, dec 2017. doi: 10.1109/robio.2017.8324448.

D. Rus and Michael T Tolley. Design, fabrication and control of soft robots. *Nature*, 521(7553):467–475, 2015.

A. Saltelli, S. Tarantola, and K. P.-S. Chan. A quantitative model-independent method for global sensitivity analysis of model output. *Technometrics*, 41(1):39–56, 1999.

A. Saltelli, S. Tarantola, and F. Campolongo. Sensitivity analysis as an ingredient of modeling. *Statistical science*, pages 377–395, 2000.

A. Saltelli, S. Tarantola, F. Campolongo, and M. Ratto. *Sensitivity analysis in practice: a guide to assessing scientific models*, volume 1. Wiley Online Library, 2004.

A. Saltelli, M. Ratto, T. Andres, F. Campolongo, J. Cariboni, D. Gatelli, M. Saisana, and S. Tarantola. *Global Sensitivity Analysis. The Primer*. Wiley, 2007. doi: 10.1002/9780470725184.

F. Schmitt, O. Piccin, L. Barbé, and B. Bayle. Soft robots manufacturing: A review. *Frontiers in Robotics and AI*, 5, jul 2018. doi: 10.3389/frobt.2018.00084.

K. Suzumori, S. Iikura, and H. Tanaka. Development of Flexible Microactuator and its Applications to Robotic Mechanisms. In *1991 IEEE International Conference on Robotics and Automation (ICRA)*, pages 1622–1627. IEEE, 1991.

J. Till, V. Aloi, and C. Rucker. Real-time dynamics of soft and continuum robots based on cosserat rod models. *The International Journal of Robotics Research*, 38(6):723–746, apr 2019. doi: 10.1177/0278364919842269.

Y. Toshimitsu, K. W. Wong, T. Buchner, and R. K. Katzschmann. Sopra: Fabrication & dynamical modeling of a scalable soft continuum robotic arm with integrated proprioceptive sensing. In *2021 IEEE/RSJ International Conference on Intelligent Robots and Systems (IROS)*, pages 653–660. IEEE, 2021. doi: 10.1109/IROS51168.2021.9636539.

D. Trivedi, A. Lotfi, and C. D. Rahn. Geometrically exact dynamic models for soft robotic manipulators. In *2007 IEEE/RSJ International Conference on Intelligent Robots and Systems (IROS)*, pages 1497–1502. IEEE, 2007. doi: 10.1109/iros.2007.4399446.

N. K. Uppalapati and G. Krishnan. Design and modeling of soft continuum manipulators using parallel asymmetric combination of fiber-reinforced elastomers. *Journal of Mechanisms and Robotics*, 13(1), oct 2020. doi: 10.1115/1.4048223.

N. K. Uppalapati, G. Singh, and G. Krishnan. Parameter estimation and modeling of a pneumatic continuum manipulator with asymmetric building blocks. In *2018 IEEE International Conference on Soft Robotics (RoboSoft)*. IEEE, apr 2018. doi: 10.1109/robosoft.2018.8405380.